Yang, H.; Huang, Y.; Gavras, S.; Kainer, K.U.; Hort, N.; Dieringa, H.:
Influences of AlN/Al Nanoparticles on the Creep Properties of Elektron21 Prepared by High Shear Dispersion Technology.
In: JOM: Journal of the Minerals, Metals and Materials Society. Vol. 71 (2019) 7, 2245 - 2252.
First published online by Springer: May 07, 2019

DOI: /10.1007/s11837-019-03499-4
https://dx.doi.org/10.1007/s11837-019-03499-4

Influences of AlN/Al nanoparticles on the creep properties of Elektron21 prepared by high shear dispersion technology

Hong Yang, Yuanding Huang, Sarkis Gavras, Karl Ulrich Kainer, Norbert Hort, Hajo Dieringa

MagIC Magnesium Innovation Centre, Helmholtz-Zentrum Geesthacht, Max-Planck Straße 1, 21502, Geesthacht, Germany

Corresponding author: hong.yang@hzg.de

Abstract

Elektron21 (E21) and its composites with additions of 0.25 wt.%, 0.5 wt.% and 1 wt.% AlN/Al nanoparticles (NPs) were fabricated by a high shear dispersion technology (HSDT). Their creep properties were investigated over a stress range between 80-140 MPa at 240 °C. The grain size exhibits an obvious increase with the addition of AlN/Al NPs compared with monolithic E21 alloy. Increasing the content of AlN/Al NPs leads to a pronounced improvement of creep resistance. Microstructural analysis shows that with the addition of 1% AlN/Al NPs in E21, the distribution of the intermetallics Mg_3RE becomes much more homogeneous and their size is reduces. Such Mg_3RE particles can prevent the dislocation slip more efficiently during creep. Besides these Mg_3RE particles, the additional formation of Al_2RE and Al_2Zr_3 phases, which results from the reactions of AlN/Al NPs and the alloying elements Zr and REs, could act as thermal stable particles to improve the creep resistance. Finally, the remained AlN NPs without reactions are beneficial for the improvement of the creep resistance to some extent due to Orowan strengthening.

1. Introduction

Magnesium (Mg)-based alloys have attracted great interests in aerospace, transportation and manufacture industries because of their light weight and specific strength. However, their wider applications are restricted due to their relatively poor creep resistance at elevated temperatures, which made them unqualified to operate in automobile transmission cases or powertrain applications up to 175 °C [1]. In order to overcome this problem, ceramic particles, such as SiC [2], Al_2O_3 [3] and AlN [4] with low density, low coefficient of thermal expansion and high thermal stability, were commonly incorporated into Mg-based alloys to enhance their creep

resistance. Especially AlN nanoparticles (NPs), with a hexagonal close packed (hcp) structure [5], were usually selected as a reinforcement in Mg matrix composites [6, 7].

The traditional preparation process, including powder metallurgy [8], high-energy ball milling [9] and stir casting [10] methods, either lack in safety or create insufficient energy to enable a uniform distribution of particles into the matrix. Ultrasonic treatment was considered as a promising economical and effective process to disperse the AlN NPs into Elektron21 (E21) alloy [4]. With this treatment, the AlN NPs could be incorporated into Mg matrix. The creep resistance of E21 with AlN NPs was improved. However, microstructural observations indicated some noticeable AlN clusters still existed in the matrix [11]. Moreover, the ultrasonic treatment is not suitable for industrial scale manufacturing. Therefore, there still exists a strong demand to search for a reliable and economical processing to fabricate the nanoparticle-reinforced Mg matrix composites (PMMCs). Recently, BCAST at Brunel university introduced a high shearing dispersion technology (HSDT) to stir the melt [12]. It can produce high energy dispersion rate to break up particle clusters and produce a better dispersion of particles. This technique was previously applied to disperse the SiC micro-sized particles in the AZ31 alloy [13]. It was found that with the assistance of HSDT the distribution of micro-sized SiC particles was quite satisfying.

In the current work, E21 is used as the base alloy, nano-sized AlN/Al NPs with the content of 0.25 wt.%, 0.5 wt.% and 1 wt.% were added for reinforcements. The creep properties of composites at 240 °C were investigated and the responsible mechanisms were explored and discussed.

2. Experimental procedures

E21 has a composition of Mg-2.85Nd-0.92Gd-0.41Zr-0.29Zn (all compositions are in wt.% hereafter unless specified) and was provided by Magnesium Elektron Ltd at Manchester, UK. Its composites were reinforced with different of AlN/Al NPs contents ranging from 0.25% to 1% fabricated by HSDT. The AlN/Al NPs with an average size of 80 nm were synthesized with aluminum (Al) wires in an argon and nitrogen atmosphere. Al wires not only reacted with nitrogen to form AlN NPs, but were also retained as metallic Al [14]. The received NPs contained 75% AlN and 25% metallic Al (here termed as AlN/Al NPs). The HSDT with a rotor-stator device, developed by BCAST at Brunel University [12, 15], was applied to disperse the AlN/Al NPs clusters [13, 16]. The device was made of a Φ 80 mm open cylinder stator and a Φ 67.5 mm motor driven rotor with 4-bladed impeller. The rotation speed can be changed from 0-3000 rpm. The detailed mechanisms and procedure can be found elsewhere [15, 17, 18].

E21 with a weight of 12 kg was molten at 720 °C in a mild steel crucible with the protective gas (Ar+1 vol% SF_6). The AlN/Al NPs with an amount of 0.25%, 0.5% and 1% were incorporated using HSDT at a rate of 3000 rpm for 1 min, respectively. After shearing, 3 kg of the molten melt was transfered into a three-zone resistance ring furnace at 670 °C for 5 min and was then immersed into a water bath at a speed of 100 mm/ min. For comparison, the as cast E21 without nanoparticle addition was also prepared.

The Vickers hardness measurements (HV5) were performed using an EMCO M1C 010 machine with a 5 kg load and a dwell time of 30 s. At least 10 indentations for each condition were made. Compression creep tests of the specimens with a dimension of Φ 6 mm and 15 mm in length were carried out at 240 °C under a constant stress between 80 and 140 MPa. Applied Test Systems (ATS) lever arm creep test systems with two thermocouples were used to evaluate the creep properties. The creep strains were measured using an extensometer connected with the measuring unit. The sample temperature evolution during creep was monitored by two thermocouples inside the chamber with an accuracy of ±1 °C. Creep experiments were interrupted once the steady-state creep stage was achieved.

The samples with a size of about 10×10×10 mm for microstructural observations were cut from cast cylinders. They were embedded in epoxy resin, which were observed along the longitudinal plane paralleled to the cooling direction. Before optical microscopy (OM) observation, samples were ground with silicon carbide abrasive paper from 500 grit to 2500 grit and were polished with oxide polishing suspension (OPS). Then an acetic-picral solution with 8 g picric acid, 5 ml acetic acid, 10 ml distilled water and 100 ml ethanol was used for etching the samples. Metallographic characterization was performed using Leica DMI5000 equipped with a digital camera and AnalySIS Pro software. Average grain size was evaluated using the linear intercept method [19] by AnalySIS Pro software. Line segments were drawn in the optical micrographs. The number of times each line segment intersects a grain boundary was counted. The average grain size was calculated as the ratio of intercept number to line length. The distribution of the grain size was determined to evaluate the uniformity degree. In order to gather quantitative grain size data, at least 50 counts were measured randomly in the optical micrographs. The number in one grain size range was divided by the total number of measured grains, and its value means the relative frequency in the whole size range. Scanning electron microscope (SEM) observations were performed using a TESCAN VEGA3-SB (Brno, Czech Republic) equipped with a Tescan energy dispersive X-ray spectrometer (EDS). Phase

identifications were performed on the high-energy X-ray beamtime HEMS P07 at PETRA III (DESY Hamburg) with wave length λ=0.01424 nm.

3. Results

3.1 Optical microstructure

The casting parameters, grain sizes and hardness of E21 and E21 reinforced with AlN/Al NPs are listed in Table I. The hardness is not significantly influenced by the addition of AlN/Al NPs ranging from 0.25% to 0.5%. With the addition of AlN/Al NPs up to 1%, the hardness shows a noticeable increase to 51.1±3.6 compared with monolithic E21 alloy (Table I). Fig. 1 shows the microstructures of as cast E21 and E21 with the addition of 0.25%, 0.5%, and 1% AlN/Al NPs by HSDT. E21 exhibits equiaxed grains with an average grain size of 80.1±5.0 μm (Fig. 1(a)). With the addition of different contents of AlN/Al NPs, the grain size shows a linear increase from 86.4±2.7 to 463.5±17.5 μm with increasing the content of AlN/Al NPs from 0.25% to 1%. E21, E21+0.25% AlN/Al and E21+0.5% AlN/Al alloys have a range of grain size from 20-300 μm. In contrast, E21+1% AlN/Al alloy has a wide range of grain size from 20-1400 μm (Fig. 1(e-h)). This indicates that the distribution of grain size is relatively uniform in the E21 with the addition of 0.25% and 0.5% AlN/Al NPs. By adding 1% AlN/Al NPs, the distribution of grain size becomes inhomogeneous, which mainly scattered in the range from 200 to 600 μm.

Table I. The casting parameters, hardness and grain size of E21 and E21 reinforced with AlN/Al NPs.

Matrix	AlN/Al [wt.%]	Stirring speed [rpm]	Stirring time [min]	Grain size [μm]	Hardness [HV5]
E21	0	-	-	80.1±5.0	45.0±1.2
E21	0.25	3000	1	86.4±2.7	46.3±2.6
E21	0.5	3000	1	144.5±4.0	45.7±2.4
E21	1	3000	1	463.5±17.5	51.1±3.6

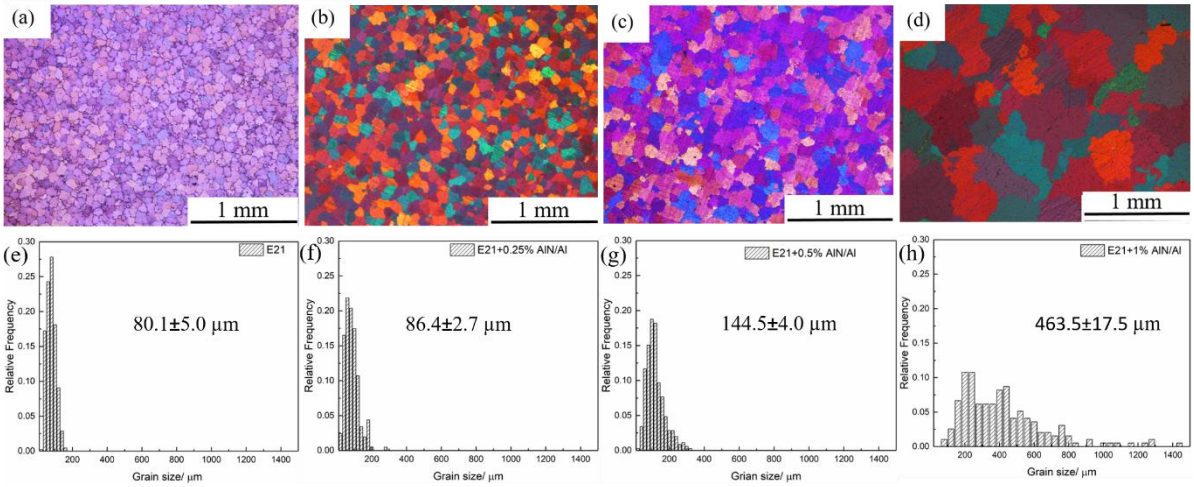

Fig. 1. Optical microstructures of as cast (a) E21, (b) E21+0.25% AlN/Al NPs, (c) E21+0.5% AlN/Al NPs, (d) E21+1% AlN/Al NPs. The corresponding grain size distribution of (a-d) are shown in (e-h), respectively.

3.2 Creep properties

Fig. 2 shows the typical curves of creep rate as a function of creep time under a stress of 80, 100, 120 and 140 MPa at 240 °C. The creep rates decrease over time for the as cast E21 and E21 composites. Table II shows the corresponding minimum creep rates of these materials. It indicates that the minimum creep rate reduces apparently with the increasing amount of AlN/Al NPs in E21 composites under all applied stress. For instance, the minimum creep rate decreases from 8.56×10^{-8} s^{-1} for E21+0.25%AlN/Al to 9.05×10^{-9} s^{-1} for E21+1%AlN/Al NPs composite under a stress of 80 MPa. With the addition of 1% AlN/Al NPs, the creep resistance was enhanced by about one order of magnitude.

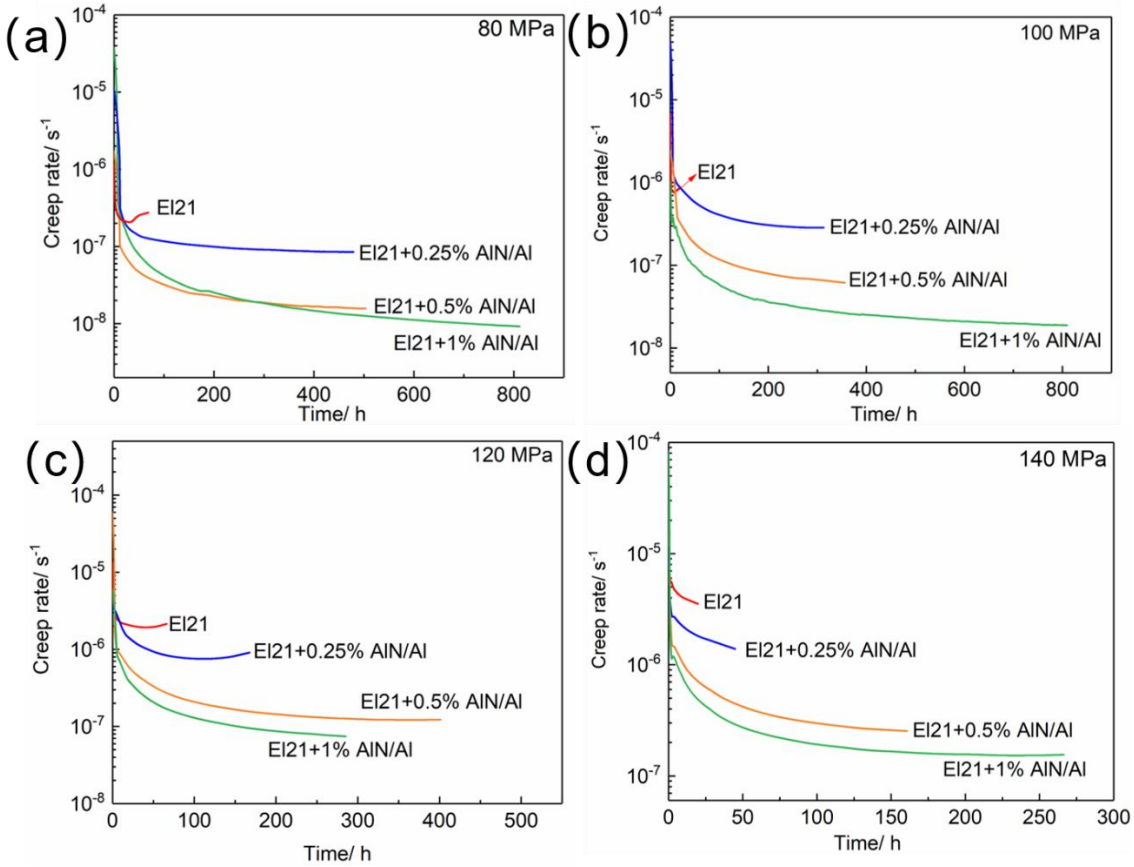

Fig. 2 Creep rate as a function of creep time at 240 °C (a) 80 MPa, (b) 100 MPa, (c) 120 MPa, (d) 140 MPa.

Table II. Minimum creep rate under different applied stresses at 240 °C. The stress exponent n was calculated by plotting the logarithmic stress vs. minimum creep rate.

	Stress [MPa]	E21	E21+0.25% NPs	E21+0.5% NPs	E21+1% NPs
	80	2.06×10^{-7}	8.56×10^{-8}	1.57×10^{-8}	9.05×10^{-9}
	100	6.87×10^{-7}	2.77×10^{-7}	6.14×10^{-8}	1.87×10^{-8}
$\dot{\varepsilon}$ [s^{-1}]	120	1.88×10^{-6}	7.5×10^{-7}	1.23×10^{-7}	7.36×10^{-8}
	140	3.68×10^{-6}	1.47×10^{-6}	2.53×10^{-7}	1.52×10^{-7}
n		5.2	5.1	4.9	5.2

Based on previous literatures [20-22], the relationship between minimum creep rate $\dot{\varepsilon}_s$ and applied stress σ can be described as Equation 1.

$$\dot{\varepsilon}_s = A\sigma^n \exp\left(-\frac{Q_C}{RT}\right) \quad (1)$$

A is a constant associated with the frequency factor and Burgers vector, σ is the applied stress, Q_c is the activation energy during creep, R is the gas constant (8.314J $mol^{-1}\cdot K^{-1}$). n is the stress exponent which implies the deformation mechanism responsible for creep. n values were calculated by the slope of $ln\dot{\varepsilon}_s$against $ln\sigma$, as Equation 2 shows.

$$\ln\dot{\varepsilon}_s = \ln A + n\ln\sigma - \frac{Q_C}{RT} \quad (2)$$

The calculated stress exponent n values were listed in Table II. They vary from 4.9 to 5.2 for these four alloys. Previous investigations indicated that n=5 is associated with dislocation climbing mechanism [23]. It can therefore be concluded the present dominant mechanism for E21 and its composites should be dislocation climbing-controlled creep.

3.3 Phase identification and SEM characterization

Fig. 3(a) shows the high-energy X-ray diffraction (XRD) patterns of as cast E21, which is mainly composed of α-Mg and Mg_3(Nd, Gd) (Mg_3RE) intermetallic compound. This result is in agreement with that reported by previous papers [11, 24, 25]. In this intermetallic compound Mg_3(Nd, Gd), Nd was partially substituted by Gd without any change of the crystal structure. It is reported Nd (r=0.1821 nm) has the similar atomic radii to Gd (r=0.1802 nm) [11]. With the addition of 0.25% AlN/Al NPs in E21, it is difficult to detect any additional peaks besides α-Mg and Mg_3RE phases (Fig. 3(b)). With further additions of AlN/Al NPs up to 0.5% and 1%, some additional peaks with relatively low intensity caused by the phases Al_2Nd and Al_2Zr_3 were identified (Fig. 3(c) and (d)).

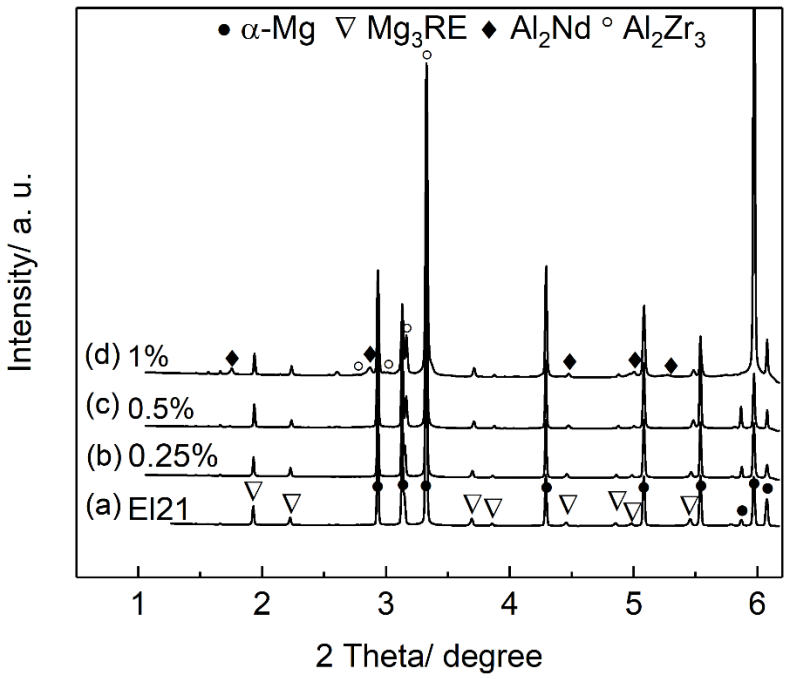

Fig. 3 High-energy XRD patterns of the as cast (a) E21 alloy, (b) E21+0.25% AlN/Al NPs and (c) E21+0.5% AlN/Al NPs and (d) E21+1% AlN/Al NPs.

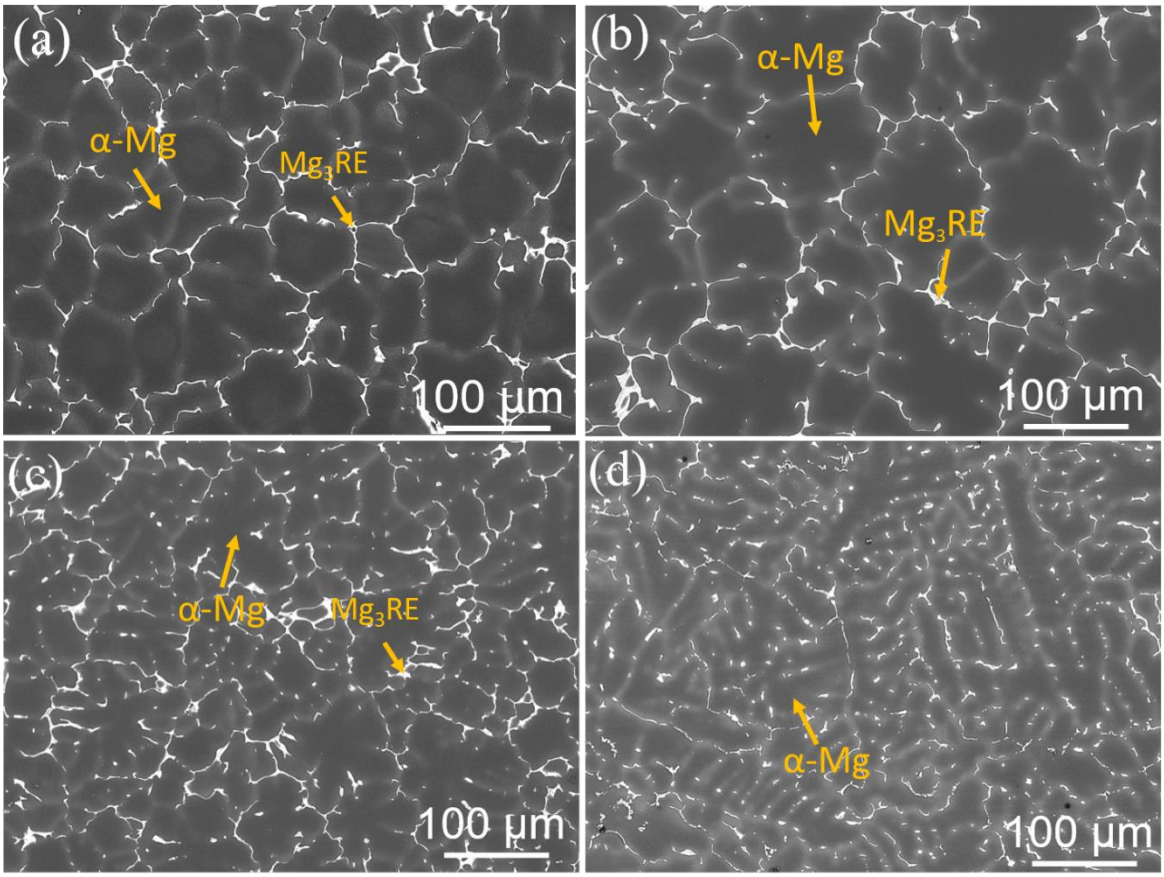

Fig. 4 Back scattered electron (BSE) SEM images of as cast (a) E21, (b) E21+0.25% AlN/Al NPs, (c) E21+0.5% AlN/Al NPs and (d) E21+1% AlN/Al NPs.

Fig. 4(a-c) shows the microstructures of as cast E21, E21+0.25% AlN/Al NPs and E21+0.5% AlN/Al NPs with α-Mg and Mg_3RE (bright phase). With the addition of AlN/Al NPs up to 1%, according to high-energy XRD results, the intermetallics are mainly composed of Mg_3RE, Al_2Zr_3 and Al_2RE phase. Without the AlN/Al NPs in E21, Mg_3RE phases are normally distributed along the dendritic boundaries (Fig. 4(a)). By adding AlN/Al NPs (Fig. 4(b-d)), the distribution of the eutectic becomes discontinuous and more homogeneous in the matrix compared with the unreinforced E21. Especially, with the addition of AlN/Al NPs up to 1%, the eutectic becomes much finer, denser and hyper-dendritic forming in the matrix.

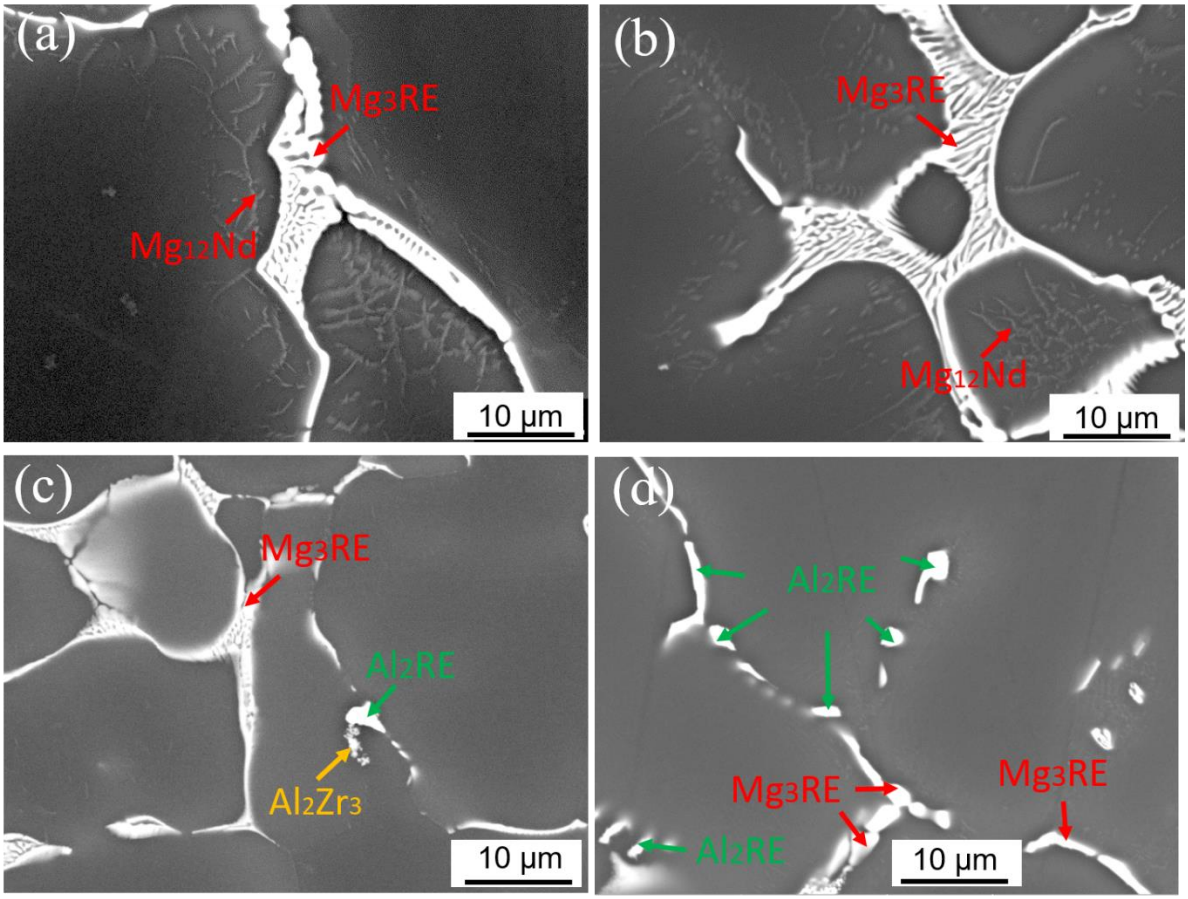

Fig. 5 BSE micrograpghs of as cast (a) E21, (b) E21+0.25% AlN/Al NPs, (c) E21+0.5% AlN/Al NPs and (d) E21+1% AlN/Al NPs.

Fig. 5(a) exhibits the lamellar Mg_3RE intermtallic phase and some lath-like precipitates located around the bright phase. These precipitates were reported to be $Mg_{12}Nd$ (tetragonal structure), which normally exist in Mg-Nd alloys due to the supersatureated of Nd [26, 27]. A

similar phenomenon was also observed in the present E21+0.25% AlN/Al NPs composites (Fig. 5(b)). After adding more AlN/Al NPs with 0.5% or 1%, the intermetallics were much refined than that of E21. Meanwhile, the $Mg_{12}Nd$ phase was difficult to be detected around the eutectic (Fig. 5(c) and (d)). This demonstrates that the addition of AlN/Al NPs influences the formation of $Mg_{12}Nd$. With increasing the content of AlN/Al NPs from 0.5% to 1%, an additional phase Al_2RE was observed (Fig. 5(c-d)). With the assistance of HSDT, it is difficult to observe any agglomerations of AlN/Al NPs in E21 with the additions of 0.25% and 0.5% AlN/Al NPs, indicating a relative homogeneous distribution of AlN/Al NPs. However, when the content of AlN/Al NPs is up to 1%, some clusters are still visible such as at P1 and P2 (Fig. 6(a)). According to the EDS mapping, P1 was confirmed as AlN NPs (Fig. 6(g) and (h)). Although the morphologies of P1 and P2 are similar (Fig. 6(b)), their contents of Zr are different. At P1 Zr element was only found in the outer layer of AlN NPs (Fig. 6(i)), implying that Zr only reacted with AlN NPs at their surfaces. Compared with P1, P2 has a much higher content of Zr. EDS point analysis also shows that besides Mg, the cluster P2 is mainly composed of Al, N and Zr (Fig. 7). All these phenomena confirm the reaction of AlN/Al NPs with Zr has happened during casting and solidification. This conclusion can further be supported by previous results that that Zr could react with AlN to form aluminides Al_2Zr and Al_3Zr at a certain temperature [28]. Besides these two aluminides, it is reported that other aluminides could also be formed. S. N. Agafonov et al. [29] reported that Al reacted with Zr to form a different stable Al_2Zr_3 phase. Based on the present results of high-energy XRD, it can be concluded that at P2 the phase Al_2Zr_3 was formed .

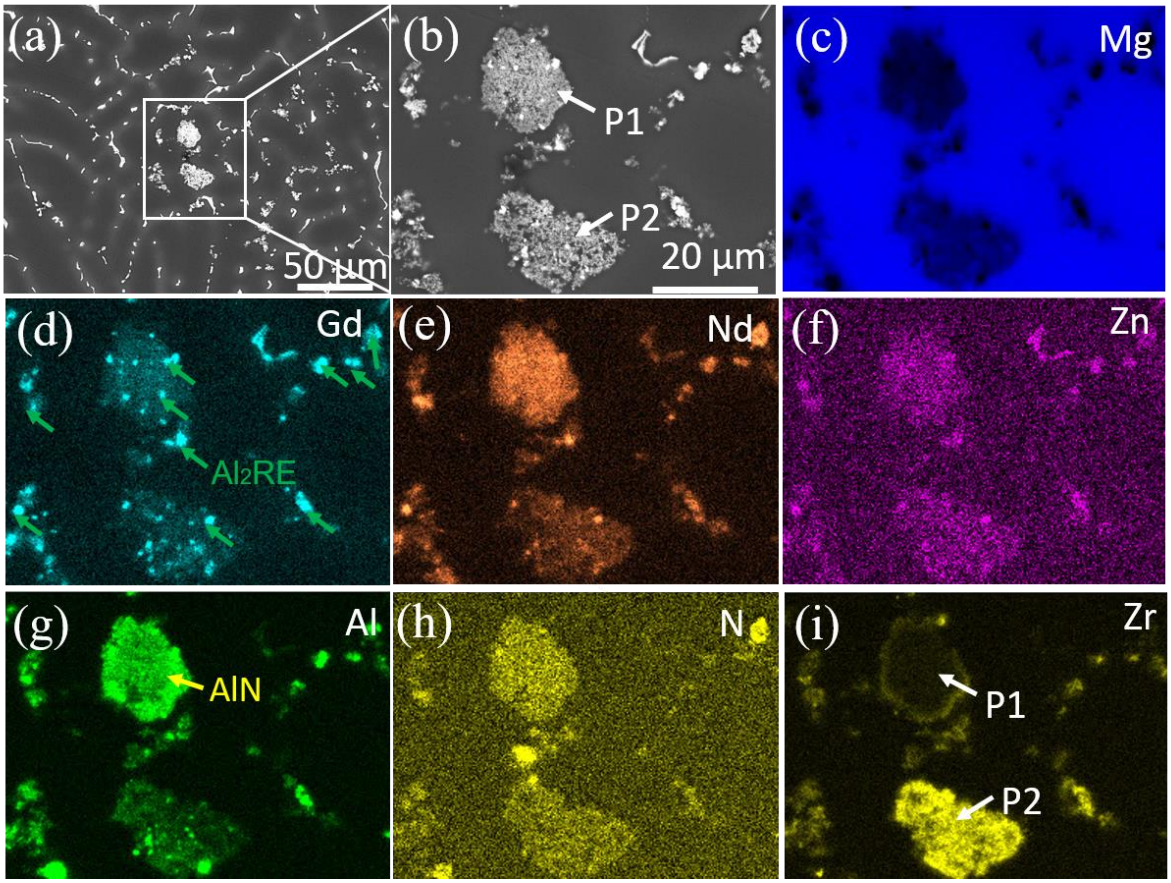

Fig. 6. (a) BSE micrograpgh of E21+1% AlN/Al NPs composite and (b) the magnified image of (a), (c-i) EDS mapping analysis of E21+1% AlN/Al NPs composite.

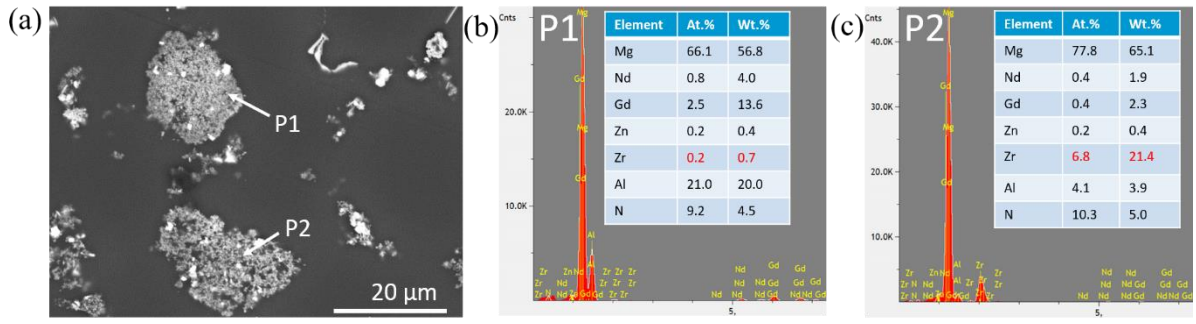

Fig. 7 BSE micrograpgh of E21+1% AlN/Al NPs composite showing the clusters of P1 and P2 and (b-c) the EDS point detection of P1 and P2 in (a).

4. Discussion

AlN NPs were usually considered as effective heterogeneous nucleation sites for the formation of α-Mg in Mg-based alloys [30]. HSDT was demonstrated to be an effective approach to refine the grain size in Mg alloys [15]. However, in the present investigation, the grain coarsening was observed with the addition of AlN/Al NPs ranging from 0.25% to 1% in

E21 using HSDT. It should be related to the poisoning mechanism of Al element in Zr-containing E21. The grain refiner Zr reacted with Al as well as AlN NPs to form the stable intermediate Al-Zr phase. Consequently, the efficiency of the grain refinement was significantly weakened by the loss of Zr. With the assistance of HSDT, the melt was intensively stirred and the possibility of contact between AlN/Al and Zr was increased. A greater amount of Zr was consequently consumed during solidification and then the grain became much larger. The identification of Al_2Zr_3 phases in the composites with the AlN/Al contents up to 0.5% and 1% further proves the loss of grain refiner Zr.

The main deformation mechanisms responsible for the second steady-state creep include dislocation creep, diffusion creep and grain boundary sliding creep [23, 31, 32]. According to the calculation of stress exponent n, it is concluded that the controlling mechanism in the AlN/Al NPs reinforced E21 composites is dislocation climbing creep. In the present investigation, the additional effects from the change of grain size on creep resistance could be ignored, since the responsible creep mechanism is dislocation climbing rather than the grain boundary sliding. This is due to the fact that at grain boundaries there exist lots of intermetallic particles such as Mg_3RE. The phases/precipitates which can hinder the dislocation movement and pin the grain/dendritic boundary sliding should be beneficial for the improvement of creep resistance at elevated temperature. In the AlN/Al NPs reinforced E21 composites, Mg_3RE phase is the main intermetallic compound, which is a thermal stable phase at the creep temperature 240 °C. It can act as an effective barrier to obstruct the dislocation movement and boundary sliding during the creep deformation. With further addition of AlN/Al NPs, the distribution of intermetallics phase becomes much more homogeneous and their size decreases. Such homogeneous and fine intermetallics can prevent the dislocation slip more efficiently during creep. Consequently, the creep resistance is improved.

The EDS mapping analysis of E21+1% AlN/Al NPs composite shows the presence of AlN clusters (Fig. 6(g)), indicating that not all the AlN NPs were consumed by the Zr. Part of AlN NPs still retained as ceramic particles in the matrix. Due to its small amount, no AlN peaks could be observed in the high-energy XRD patterns. According to Orowan strengthening [33], these remained NPs can hinder the dislocation movement, especially for these particles with small size and relative homogeneous distribution. Therefore, the AlN NPs can contribute to the improvement of creep resistance to some extent.

With increasing the content of AlN/Al NPs from 0.5% to 1%, the amount of Al_2RE also increased (Fig. 5(c-d)). They are interconnected with Mg_3RE to occupy the dendritic boundaries in the matrix. Amberger et al. [34] investigated MRI230D alloy and found that the highly connected secondary phase Al_2Ca along the boundaries enhances the creep resistance because they can effectively shield load from the soft α-Mg matrix. It is believed that the formation of Al_2RE caused by the reaction of Al with REs also contribute to the improvement of creep resistance for the AlN/Al NPs reinforced E21 composites. Normally, the thermal stability of intermetallics is proportional to their melting points, the higher their melting point the higher their thermal stability. The melting point of Al_2RE is 1200 °C which is much higher than that of Mg_3RE (780 °C) [35], implying it has a better thermal stability than Mg_3RE. Zhu et al. [36] also reported that Al_2RE was stable at temperatures up to 200 °C without any distinct decomposition. Al_2RE may provide positive effects on the improvement of creep resistance at elevated temperatures to some extent. Moreover, although its amount is small, the formation of Al_2Zr_3 phase may be also beneficial for the improvement of creep properties. Kabirian et al [37] reported that the creep resistance of AZ91 with the addition of Zr in the range of 0.2-1.0 wt.% were enhanced significantly due to the occurrence of Al-Zr intermetallics. Al-Zr intermetallic particles could act as thermal stable particles to oppose the revery process. In summary, the increase in the fraction of the intermetallic phases as a result of the reaction of AlN/Al NPs with the alloying elements RE and Zr that is helpful for the improvement in creep resistance.

Conclusions

The E21 composites reinforced with 0.25%, 0.5% and 1% AlN/Al NPs reinforced E21 composites were successfully prepared by HSDT. The following conclusions can be drawn:

1. The grain size exhibits an obvious increase in AlN/Al NPs reinforced E21 composites compared with monolithic E21. With increasing content of the AlN/Al NPs, the grain becomes larger. This is attributed to the poison mechanism of Al addition in this Zr-containing E21.
2. The creep resistance is improved for the E21 with the addition of AlN/Al NPs. With the addition of 1% AlN/Al NPs, the creep resistance increases by more than one order of magnitude. The responsible strengthening mechanism is mainly ascribed to the homogeneous and refined intermetallics at dendritic boundaries. They can inhibit dislocation movement more effectively during creep.

3. The formation of additional Al_2RE and Al_2Zr_3 phases by the reaction of AlN/Al NPs and the alloying elements REs and Zr can contribute to the improvement of creep resistance. Meanwhile, the remained AlN NPs without reaction are also beneficial for improving the creep resistance due to Orowan strengthening.

Acknowledgement

The authors acknowledge Mr. G. Meister and Mr. Yiming Jin for preparing the alloys. Hong Yang gratefully thanks the China Scholarship Council (201606050110) for the award of a fellowship and funding.

References

[1] A.A. Luo, *Int. Mater. Rev.* 49 13 (2004).
[2] F. Labib, R. Mahmudi, H.M. Ghasemi, *Mater. Sci. Eng., A* 640 91 (2015).
[3] H. Dieringa, Y. Huang, P. Maier, N. Hort, K.U. Kainer, *Mater. Sci. Eng., A* 410-411 85 (2005).
[4] L. Katsarou, M. Mounib, W. Lefebvre, S. Vorozhtsov, M. Pavese, C. Badini, J.M. Molina-Aldareguia, C.C. Jimenez, M.T. Pérez Prado, H. Dieringa, *Mater. Sci. Eng., A* 659 84 (2016).
[5] H.M. Fu, M.X. Zhang, D. Qiu, P.M. Kelly, J.A. Taylor, *J. Alloys Compd.* 478 809 (2009).
[6] E. Bedolla, J. Lemus-Ruiz, A. Contreras, *Mater. Des.* 38 91 (2012).
[7] S. Sankaranarayanan, M.K. Habibi, S. Jayalakshmi, K. Jia Ai, A. Almajid, M. Gupta, *Mater. Sci. Technol.* 31 1122 (2014).
[8] S.F. Hassan, M. Gupta, *Mater. Sci. Eng., A* 392 163 (2005).
[9] S. Kamrani, D. Penther, A. Ghasemi, R. Riedel, C. Fleck, *Adv. Powder Technol.* 29 1742 (2018).
[10] K.B. Nie, X.J. Wang, K. Wu, L. Xu, M.Y. Zheng, X.S. Hu, *J. Alloys Compd.* 509 8664 (2011).
[11] A. Saboori, E. Padovano, M. Pavese, H. Dieringa, C. Badini, *Materials (Basel)* 10 (2017).
[12] S. Tzamtzis, H. Zhang, N. Hari Babu, Z. Fan, *Mater. Sci. Eng., A* 527 2929 (2010).
[13] X. Yang, Y. Huang, N.S. Barekar, S. Das, I.C. Stone, Z. Fan, *Composites, Part A* 90 349 (2016).
[14] M.I. Lerner, E.A. Glazkova, A.S. Lozhkomoev, N.V. Svarovskaya, O.V. Bakina, A.V. Pervikov, S.G. Psakhie, *Powder Technol.* 295 307 (2016).
[15] Z. Fan, Y. Wang, M. Xia, S. Arumuganathar, *Acta Mater.* 57 4891 (2009).
[16] J.B. Patel, X. Yang, C.L. Mendis, Z. Fan, *JOM* 69 1071 (2017).
[17] Z. Fan, G. Liu, *Acta Mater.* 53 4345 (2005).
[18] H. Men, B. Jiang, Z. Fan, *Acta Mater.* 58 6526 (2010).
[19] A. Standard, *Standard Test Method for Determining Average Grain Size." West Conshohocken, PA* 1 (2013).
[20] H. Dieringa, *J. Mater. Sci.* 46 289 (2011).
[21] H. Dieringa, Y. Huang, P. Wittke, M. Klein, F. Walther, M. Dikovits, C. Poletti, *Mater. Sci. Eng., A* 585 430 (2013).
[22] A. Arunachaleswaran, I.M. Pereira, H. Dieringa, Y. Huang, N. Hort, B.K. Dhindaw, K.U. Kainer, *Mater. Sci. Eng., A* 460-461 268 (2007).
[23] H. Somekawa, K. Hirai, H. Watanabe, Y. Takigawa, K. Higashi, *Mater. Sci. Eng., A* 407 53 (2005).
[24] A. Saboori, E. Padovano, M. Pavese, C. Badini, *Materials (Basel)* 11 (2017).
[25] A. Kielbus, T. Rzychon, R. Przeliorz, *Mater. Sci. Forum* 638-642 1447 (2010).
[26] L. Peng, P. Fu, Z. Li, Y. Wang, H. Jiang, *J. Mater. Sci.* 49 7105 (2014).
[27] D. Wu, Y.Q. Ma, R.S. Chen, W. Ke, *J. Magnesium Alloys* 2 20 (2014).
[28] J.M.A.P.a.J.P. Abriata, *Phase Diagram Evaluations: Section II* 13 277 (1992).
[29] S.N. Agafonov, S.A. Krasikov, A.A. Ponomarenko, L.A. Ovchinnikova, *Inorg. Mater.* 48 813 (2012).

[30] H.M. Fu, M.X. Zhang, D. Qiu, P.M. Kelly, J.A. Taylor, *J. Alloys Compd.* 478 809 (2009).
[31] N. Mo, Q. Tan, M. Bermingham, Y. Huang, H. Dieringa, N. Hort, M.-X. Zhang, *Mater. Des.* 155 422 (2018).
[32] K.R. Athul, U.T.S. Pillai, A. Srinivasan, B.C. Pai, *Adv. Eng. Mater.* 18 770 (2016).
[33] J.B. Ferguson, F. Sheykh-Jaberi, C.-S. Kim, P.K. Rohatgi, K. Cho, *Mater. Sci. Eng., A* 558 193 (2012).
[34] D. Amberger, P. Eisenlohr, M. Göken, *Acta Mater.* 60 2277 (2012).
[35] N. Hort, Y. Huang, K.U. Kainer, *Adv. Eng. Mater.* 8 235 (2006).
[36] S.M. Zhu, J.F. Nie, M.A. Gibson, M.A. Easton, P. Bakke, *Metall. Mater. Trans. A* 43 4137 (2012).
[37] F. Kabirian, R. Mahmudi, *Metall. Mater. Trans. A* 41 3488 (2010).